Control of a flexible, surface-piercing hydrofoil for high-speed, small-scale applications

Control of a flexible, surface-piercing hydrofoil for high-speed, small-scale applications

Gabriel D. Bousquet, Michael S. Triantafyllou and Jean-Jacques E. Slotine

***Abstract*— In recent years, hydrofoils have become ubiquitous and critical components of high-performance surface vehicles. Twenty-meter-long hydrofoil sailing craft are capable of reaching speeds in excess of 45 knots. Hydrofoil dinghies routinely travel faster than the wind and reach speeds up to 30 knots. Besides, in the quest for super-maneuverability, actuated hydrofoils could enable the efficient generation of large forces on demand. However, the control of hydrofoil systems remains challenging, especially in rough seas. With the intent to ultimately enable the design of versatile, small-scale, high-speed, and super-maneuverable surface vehicles, we investigate the problem of controlling the lift force generated by a flexible, surface-piercing hydrofoil traveling at high speed through a random wave field. We present a test platform composed of a rudder-like vertical hydrofoil actuated in pitch. The system is instrumented with velocity, force, and immersion depth sensors. We carry out high-speed field experiments in the presence of naturally occurring waves. The 2 cm chord hydrofoil is successfully controlled with a LTV/feedback linearization controller at speeds ranging from 4 to 10+ m/s.**

I. Introduction

The last decades have seen a vigorous development of autonomous, small-scale ocean surface and underwater vehicles [1], [2], [3], [4], as they are low-cost and can be deployed in large numbers. A general drawback of small-scale surface and underwater vehicles is their relative low speed. In particular, surface vehicles in motion generate a wake of surface gravity-waves with their hulls [5], which represent an additional source of drag. The important non-dimensional parameter for characterizing wave-making is the Froude number $F_r = U/\sqrt{gL}$ where U is the vehicle speed and L is the length of the hull. Typically, wave drag is significant in the region $0.1 \lesssim F_r \lesssim 1$ and peaks around $F_r \sim 0.4-0.5$ [6]. The so-called "hull speed" $U = 0.4\sqrt{gL}$, associated with this special Froude number, is a loose analog of the speed of sound for surface vehicles: unless they have been specifically designed, as a rule of thumb ships do not exceed their hull speed. The hull speed increases with the square root of the ship length, *de facto* imposing a stringent speed limit on small-scale surface vehicles with a hull.

An alternative way to generate hydrodynamic forces is by means of hydrofoils [7], [8]. They may be horizontal for weight compensation, vertical for lateral maneuvering, or a combination of both. Hydrofoil surface vehicles are experiencing a rapid development, in particular among recreational and competitive sailboats [9], [10], [11], ranging from 2 m to 20 m in length. When they reach high speeds, those boats "take off" such that the hull is not in contact with the water, only their hydrofoils interact with it. The physics of hydrofoils is only weakly affected by their scale—provided that the Reynolds number $R_e = Uc/\nu$ remains larger than $\sim 10^5$—such that small systems are not penalized by their size. For instance, the small "hydrofoil moth" dinghy, while only 3.5 m in length, has been recorded to travel at 14 m/s, almost 75% of the 20 m/s reached by the 22 m long America's cup AC72s.

Fig. 1. Pitch-actuated, 2 cm chord surface-piercing hydrofoil for high-speed applications. In this experiment the hydrofoil is towed at 10 m/s.

A biological example of a hydrofoil surface system is the flying fish [12] pictured in Figure 2. The 20–30 cm long fish is most famous for executing long gliding flights above the water (up to 400 m out of the water in a sequence of 50 m glides). These flights are powered by a 10–20 m "taxiing phase" where the body of the fish is out of the water but its caudal fin is partially in the water. There, the fish flaps its tail and accelerates from 8–10 m/s up to 15–20 m/s, when it takes off for the glide. In the taxiing phase, the fish's

Department of Mechanical Engineering, Massachusetts Institute of Technology, Cambridge, MA 02139, USA; {g_b,mistetri,jjs}@mit.edu

This work was partially funded by a Link Ocean Engineering and Instrumentation fellowship.

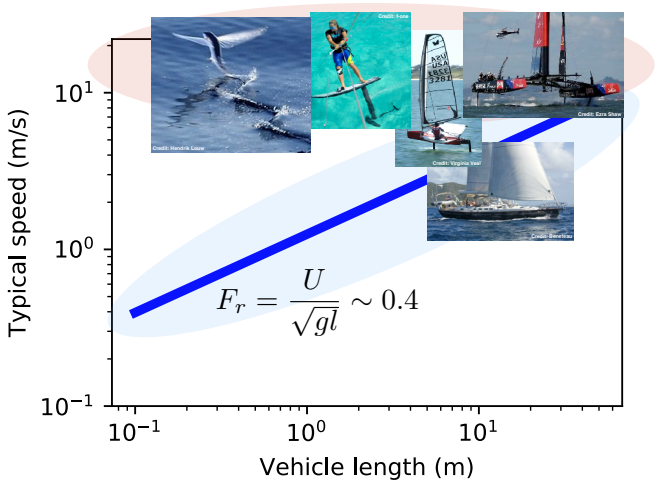

Fig. 2. Comparison between hull speed and hydrofoil-based surface vehicles across scales.

only connection to the water is the caudal fin *i.e.* a flapping, vertical, surface-piercing hydrofoil used for propulsion. This makes the flying fish in taxi phase a hydrofoil surface craft. Overall, hydrofoils appear to be features of choice for small-scale, high-speed surface vehicles, and more generally for bio-inspired and super-maneuverable ocean robots.

In general, the hydrodynamics of surface-piercing hydrofoils is a complex topic of active research [7], [8], [13], as it may concurrently involve free-surface effects (wave-making), ventilation (air from the surface is entrained into the suction side of the hydrofoil, resulting in a sudden loss of lift and increase in drag, see [14], [13] and Figure 8), and cavitation (at high speed, water may boil in regions of low pressure). Active control of hydrofoils has mostly focused on fully submerged systems and remains challenging, especially in rough seas [15].

Small-scale surface-piercing hydrofoils, designed to generate lift forces $O(10$ N$)$ at velocities $O(10$ m/s$)$, present unique characteristics and challenges that remain largely unexplored. Due to their small size, even the smallest wave has a proportionally big effect on their wetted area, leading to fast and large amplitude forcing, and a highly time-varying dynamics. This can be mitigated somehow by utilizing long, slender hydrofoils, but these are inherently flexible.

In this paper, we investigate the control of the lift force (more precisely, the measured torque, thereafter lumped under the generic term "loading"), generated by a vertical, rectangular surface-piercing hydrofoil actuated in pitch. We derive a general model of the hydrofoil dynamics and propose a linear time-varying (LTV) controller. The controller is validated on a 2 cm chord hydrofoil, immersed by 0–20 cm. The hydrofoil is sized for a design lift of 5 N at a travel speed of 10 m/s. Tests are carried at speeds 4–10+ m/s in an outdoor basin with naturally occurring waves.

II. Experimental setup

The experimental setup (Figure 1) was designed for a 2×20 cm hydrofoil ("foil" for short) that was towed with a 40 hp whaler boat capable of speeds up to 12 m/s. Experiments were carried on the Charles River basin near MIT, during Summer 2016. Given the size of the basin (2 km) and safety requirements, the test runs were typically 60–100 second long. As shown in Figure 1, the natural water surface on which the experiment were carried out had some waves of typical height ~ 5 cm and wavelength ~ 2 m, due to winds and the wakes of other craft. Besides, the natural pitching and heaving motion of the boat was also ~ 5 cm at a frequency $\sim 1/3$ Hz, as it was traveling at high speed and forced by waves.

A. Hydrofoil system

The hydrofoil system, shown in Figure 1, a component for a future high-speed surface autonomous vehicle, is a carbon fiber composite, off-the-shelf helicopter blade (Zeal 210 mm). It has a nearly constant chord, and an unknown profile. When loaded at the tip, the hydrofoil has a strength of approximately 15 N and a stiffness of 13 Nm/rad.

The hydrofoil is pitch-actuated in direct drive mode by a high-speed model helicopter servo (MKS HV93i) through a rigid shaft. The custom-engineered shaft-foil connector is instrumented with strain gauges in a full-bridge configuration, in order to measure and control the loading generated by the hydrofoil.

The system's velocity is measured at 10 Hz by GPS (u-blox M8) and the hydrofoil depth of immersion is measured at 40 Hz by a downward-facing ultrasonic rangefinder (MaxBotix 7047).

The sensing, control, communication and logging are performed with a Lisa-MX/Paparazzi autopilot [16], [17]. The GPS and sonar communicate with the autopilot via Serial and I2C. The strain gauge signal is pre-amplified with a custom-engineered amplification stage and read by the 12 bit ADC of the microcontroller. The amplification gain is set up such that the resolution of the load measurement is approximately 300 ADC counts for 1 Nm. The autopilot is connected by USB to a laptop on the boat for real-time data logging. The autopilot is also commanded via a hobbyist 2.4 GHz RC-controller.

B. Test rig

A custom-engineered rig is secured to the whaler boat (Figure 3). The hydrofoil system is located at the end of a ~ 2 m cantilever beam, which can be manually positioned away from the boat wake and adjusted in pitch. A push-pull rope system allows for a manual adjustment of the hydrofoil immersion depth. Because the rig is a cantilever beam, small amplitude but lightly damped vibration modes exist at ~ 3 Hz in heave and ~ 1.5 Hz in surge, respectively.

III. Modelization and parameterization

We consider the surface-piercing hydrofoil of Figure 1, whose base is traveling at speed U (perhaps slowly varying) along $-\mathbf{e}_x$ (without waves, the flow would be coming at the vehicle at $+U\mathbf{e}_x$). The small-angle foil pitch is θ. Its beam and chord are b, c, respectively. The foil flexibility is modeled

Fig. 3. Test rig and hydrofoil system, secured on the whaler boat. Left: the apparatus is being configured at the dock. Right: Ongoing hydrofoil experiment. As the arrows show, the rig allows for manual positioning of the hydrofoil in three directions: the beam itself can be translated away from the boat wake and pivoted in pitch. Furthermore, the hydrofoil can he lowered or lifted in real-time by push-pulling the red and blue lines.

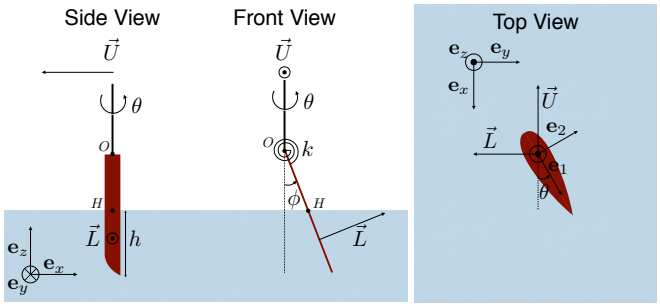

Fig. 4. Hydrofoil model and parameterization. The hydrofoil flexibility is modeled by a torsional spring of stiffness k. Its immersion depth h is time-varying due to surface waves (not drawn).

by a hinge at its base, of stiffness k and negligible damping. The foil is immersed at a depth $h(t) \leq b$. Its bending is parameterized by the small hinge angle ϕ. We assume that the bending is measured (in the present experiments, strain gauges were installed on the hydrofoil).

The foil dynamics is

$$J\ddot{\phi} = M_{\text{hinge}} + M_{\text{a.m.}} + M_L \tag{1}$$

where J is the foil's inertia measured at the hinge and the terms on the right-hand side are the moment due to the hinge stiffness $M_{\text{hinge}} = -k\phi$, hydrodynamic added mass, and lift, respectively.

A. Sea state and hydrodynamic relative velocities

We assume the presence of a wave field of small orbital velocity $\mathbf{u}(\mathbf{x}, t) = (u_x, u_y, u_z)$. The relative hydrodynamic speed of a point M at the quarter-chord of the hydrofoil, at a height z above the tip, is

$$\mathbf{V}_{\text{rel}} = U\mathbf{e}_x + \mathbf{u} - \frac{d}{dt}\mathbf{OM} \text{ with } \mathbf{OM} = \begin{bmatrix} -\phi(b-z)\sin\theta \\ \phi(b-z)\cos\theta \\ -(b-z)) \end{bmatrix}$$

from which the relative velocity magnitude and direction can be computed. To the dominant order, the relative velocity magnitude is $V_{\text{rel}}^2 \approx U^2 + 2Uu_x$, and the relative direction (angle of the flow) is $\alpha_{\text{flow}} \approx \frac{u_y}{U} - (b-z)\frac{\dot{\phi}}{U}$. In the following, we define the hydrodynamic pressure $q = \frac{1}{2}\rho V_{\text{rel}}^2$ where ρ is the density of water.

B. Added mass

The added mass forces are computed using slender body theory along the z-axis [5]. For a thin airfoil, the cross section area is small, and the only significant added mass coefficient or interest is $m_{22} \approx \pi c^2/4$. Under those hypotheses, the element of force perpendicular to the hydrofoil (direction of vector $\mathbf{e}_2$, see Figure 4) is

$$\begin{aligned} dF_2 &= -m_{22}\frac{d}{dt}(\mathbf{V}_{\text{rel}}.\mathbf{e}_2)dz \\ &\approx m_{22}(U\dot{\theta} - \dot{u}_y + (b-z)\ddot{\phi})dz. \end{aligned} \tag{2}$$

Within this approximation, the moment on the foil due to added mass is

$$\begin{aligned} M_{\text{a.m.,flat}} &= -\int_0^h (b-z)\frac{dF_2}{dz}dz \\ &= m_{22}h\left(\lambda(\dot{u}_y - U\dot{\theta}) - \sigma\ddot{\phi}\right) \end{aligned} \tag{3}$$

with $\lambda = b - h/2$ and $\sigma = \lambda^2 + h^2/12$ (both time-dependent if h is). Note that for $h/b \lesssim 1/2$, $\sigma \approx \lambda^2$.

Furthermore, there is an extra added mass term in the presence of waves, due to their diffraction and radiation. While a full treatment of the small forces incurred is beyond the scope of this paper, the following approximation can be used:

$$M_{\text{a.m.,wave}} \approx -\frac{m_{22}}{2}\dot{h}u_y(h-b). \tag{4}$$

Finally, the total moment due to added mass effects is modeled as $M_{\text{a.m.}} = M_{\text{a.m.,flat}} + M_{\text{a.m.,wave}}$.

C. Lift

Consider only the immersed part or the hydrofoil, and H the point of the foil that is at the water surface at time t. The local angle of attack at that point is $\alpha_H = \theta + (\dot{\phi}(b-h) + u_y)/U$. The force and moment at point H on the hydrofoil due to hydrodynamic lift are

$$\begin{aligned} L &= qch(C_{L,\alpha}\alpha_H + C_{L,p'}\dot{\phi}h/(2U)) \\ M_H &= qch^2(C_{l,\alpha}\alpha_H + C_{l,p'}\dot{\phi}h/(2U)) \end{aligned} \tag{5}$$

where $C_{L,\alpha}$ and $C_{L,p'}$ are the force coefficients due to angle of attack and roll rate, respectively, and $C_{l,\alpha}$ and $C_{l,p'}$ are the moment coefficients due to angle of attack and roll rate, respectively [18]. In general, the hydrodynamic coefficients are non-trivial. Due to surface wave-making effects they are strongly dependent on the Froude number $F_r = U/\sqrt{gc}$ [19], [20]. In practice, for $F_r \lesssim 0.1$ or $F_r \gtrsim 1$, the dependence is weak, and the coefficients are mostly sensitive to the immersed aspect ratio $\mathcal{AR} = h/c$. For $F_r \to \infty$, the flow can be solved with the method of images where the horizontal surface plane is anti-symmetric [5], and the coefficients may be computed with a panel method such as AVL [21]. In the present study, the hydrodynamic coefficients were computed and fitted with a third order polynomial (Figure 5). Finally, the moment due to lift at the hinge is $M_L = (b-h)L + M_H$, which can be rewritten as

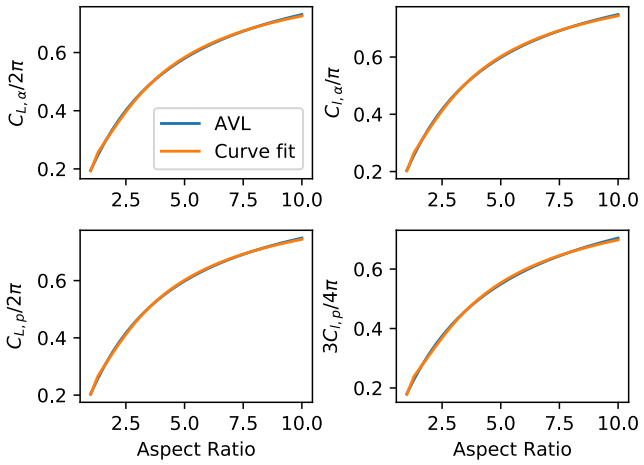

X	c_0	c_1	c_2	c_3
$C_{L,\alpha}$	5.71	−12.9	14.5	−6.15
$C_{l,\alpha}$	2.91	−6.39	7.09	−2.97
$C_{L,p'}$	5.82	−12.8	14.2	−5.94
$C_{l,p'}$	3.71	−8.85	10.4	−4.51

Fig. 5. Hydrodynamic coefficients obtained with AVL as a function of the aspect ratio $\mathcal{AR} = h/c$, fitted with a third order polynomial of the form $X = c_0 + c_1/\mathcal{AR} + c_2/\mathcal{AR}^2 + c_3/\mathcal{AR}^3$ in the range $1 \leq \mathcal{AR} \leq 10$. Note in the plots the analytic limit for $\mathcal{AR} \to \infty$.

$$M_L = qch^2 C_{M,\theta}(\theta + u_y/U) + \frac{qch^3}{U} C_{M,\dot{\phi}} \dot{\phi} \tag{6}$$

with

$$\begin{aligned} C_{M,\theta} &= \hbar C_{L,\alpha} + C_{l,\alpha} \\ C_{M,\dot{\phi}} &= \hbar^2 C_{L,\alpha} + \hbar C_{l,\alpha} + \hbar C_{L,p'} + C_{l,p'} \end{aligned} \tag{7}$$

and $\hbar = (b/h - 1)$.

D. Other hydrodynamic forces

The lift coefficients are valid if there is no ventilation. In the presence of stable and full ventilation, it is also possible to compute coefficients, different from those of Figure 5. Drag forces (including a small spray drag), may be present but they have a negligible effect on the foil bending as they are parallel to the flow. Finally, at high speeds ($U \gtrsim 20$ m/s), cavitation may also alter lift and drag.

E. Dynamics

Collecting all terms, the hydrofoil dynamics is

$$a_{\ddot{\phi}} \ddot{\phi} + a_{\dot{\phi}} \dot{\phi} + a_\phi \phi = b_\theta \theta + b_{\dot{\theta}} \dot{\theta} + r(t) \tag{8}$$

where the coefficients

$$\begin{aligned} a_{\ddot{\phi}} &= J + m_{22} h \sigma, \qquad a_{\dot{\phi}} = \frac{qch^3}{U} C_{M,\dot{\phi}}, \qquad a_\phi = k \\ b_\theta &= qch^2 C_{M,\theta}, \qquad b_{\dot{\theta}} = -m_{22} h \lambda U \end{aligned} \tag{9}$$

are time-varying, and

$$r(t) = m_{22} h \lambda \dot{u}_y - m_{22}(h - b) \dot{h} u_y / 2 + qch^2 C_{M,\theta} u_y / U$$

can be considered as high-frequency noise.

IV. Control

A. Control objectives

The control objectives consist of 1) maintaining at all times the loading of the hydrofoil below its strength limit, 2) performing robust following of a commanded loading $k\phi_m(t)$ despite fast and order-of-magnitude variations of the plant due to variations in U and h, and 3) performing noise rejection while maintaining the error within acceptable limits. For instance, assuming that the roll φ of the vehicle on which the hydrofoil is to be mounted has a known linear dynamics of the form $\varphi = H(s) k\tilde{\phi}$ where $k\tilde{\phi}$ is the loading error, a bound on the allowed error in the vehicle roll constrains the allowable spectrum of the loading error. This particular hydrofoil system is designed for a vehicle whose roll dynamics is dominated by damping such that $H(s) = 0.03/s$ with a maximum allowable roll $|\varphi| \leq 2°$.

B. Simplified foil equations for control

In coefficient $a_{\ddot{\phi}}$, the added mass term $m_{22} h \sigma$ typically dominates the material inertia J by over one order of magnitude. Therefore, $a_{\dot{\phi}}/a_{\ddot{\phi}} \sim b_\theta/b_{\dot{\theta}} \sim U/c$. For small-scale, high-speed applications, the ratios may be in the 500s to 1000s rad/s, much faster than *e.g.* unmodeled pitch actuator dynamics. Therefore, it is a sensible approximation to ignore, for control, the terms $a_{\ddot{\phi}} \ddot{\phi}$ and $b_{\dot{\theta}} \dot{\theta}$, such that a good approximation for the hydrofoil system is simply

$$a_{\dot{\phi}}(t) \dot{\phi} + a_\phi(t) \phi = b_\theta(t) \theta \tag{10}$$

which is a first-order LTV system. Note that the plant "pole" $a_\phi/a_{\dot{\phi}}$ may vary by one order of magnitude over the course of an experiment and the "gain" b_θ/a_ϕ may vary by two orders of magnitude, as the hydrofoil's immersion h varies between 0 and 20 cm, and the velocity U ranges from 4 to 10 m/s.

C. Controller

We use a LTV/feedback linearization controller, as it allows to address the fast-changing but well-modeled properties of the plant, without sacrificing simplicity:

$$\hat{h} = \frac{1}{\left(s^2/p_{\text{sonar}} + \sqrt{2} s/p_{\text{sonar}} + 1\right)^2} h_{\text{sonar}} \tag{11a}$$

$$\hat{U} = \frac{1}{s/p_U + 1} U_{\text{GPS}} \tag{11b}$$

$$\hat{a}_{\dot{\phi}}, \hat{a}_\phi, \hat{b}_\theta \quad \text{formed from } \hat{h}, \hat{U} \text{ and Eq. (9)} \tag{11c}$$

$$\phi_m = \frac{1}{(s/\lambda + 1)^2} \phi_r \tag{11d}$$

$$\tilde{\phi} = \phi - \phi_m \tag{11e}$$

$$\dot{I} = \tilde{\phi} \quad (c.f. \text{ Fig. 6}) \tag{11f}$$

$$\theta = \frac{\eta \hat{a}_\phi}{\hat{b}_\theta} \phi + \frac{\hat{a}_{\dot{\phi}}}{\hat{b}_\theta} \left(\dot{\phi}_m - 2\beta \tilde{\phi} - \beta^2 I \right) \tag{11g}$$

The controller is implemented by Euler integration at 512 Hz. In equations (11a) and (11b), the estimates for the immersion depth and vehicle velocity $\hat{h}$ and $\hat{U}$ are obtained by filtering the noisy sonar and GPS velocity measurements and used

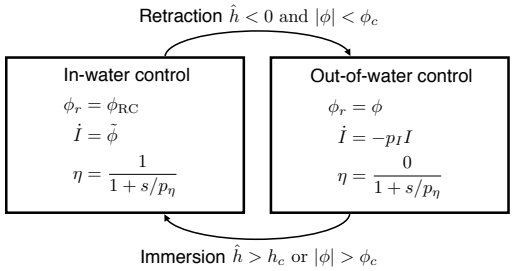

Fig. 6. Out-of-water and in-water modes. Transitions between the modes are computed with respect to depth immersion and load criteria. $h_c = 2$ cm is a small depth immersion threshold and ϕ_c corresponds to a safety loading above which control should be applied independently of the depth readings.

to compute the time-varying coefficients of Equation (10). The sonar is operated at 40 Hz with $p_{\text{sonar}} = 12$ s^{-1}, and the GPS at 10 Hz with $p_{\text{U}} = 1$ s^{-1}. When the hydrofoil is immersed, the reference loading ϕ_r in Equation (11d) is directly read from manual remote controller stick input ϕ_{RC}. In equations (11e-g), the error signals are computed and the control law is formed. In the absence of waves, the control system is stable by design. Indeed in that case the system reduces to $(s+\beta)^2 \int \tilde{\phi} = 0$ because $\eta = 1$ and $\hat{a}_i = a_i, \hat{b}_\theta = b_\theta$. Besides, the stability is robust in the sense that in the presence of small waves (small error in Equation (9)), it is straightforward to show with a Lyapunov linear-quadratic method that stability is maintained. Moving forward, sliding or adaptive control may improve the performance and robustness of the controller.

Note the integral aspect of the controller is important as due to misalignments of the rig, θ has a significant unknown bias. Besides the noise due to wave forcing, another important dynamics not modeled in Eq. (10) is the servo, which can be approximated as a rate-limited, critically-damped second-order system of poorly known cutoff rate p_{servo} in the 20-60 s^{-1} range. It was determined that $\beta = 10$ s^{-1} offered a good performance/robustness trade-off (8 dB gain margin and 50° phase margin for $a_\phi/a_{\dot{\phi}} = 15$ s^{-1} and $p_{\text{servo}} = 40$ s^{-1}).

D. Hydrofoil immersion and retraction

Because of waves, vehicle dynamics and/or vehicle reconfiguration, it is expected that the hydrofoil should transition frequently between immersed and fully out-of-water phases. This is a potential issue since if the hydrofoil enters the water with a large pitch, large transient forces occur. Furthermore, large pitch, especially upon entry, is conducive to ventilation [14], an undesirable phenomenon since it is associated with decreased lift and increased drag. Besides, ventilation is difficult to model. In particular, it is often bi-stable (in a given configuration, both the ventilated and non-ventilated states may occur), and the inception of ventilation has a much faster dynamics than its closure. In order to ensure that the angle of attack upon entry is small, foil immersion and retraction was monitored with the sonar and the state machine logic of Figure 6 was applied. It ensured smooth control during transitions in and out of the water. When the foil is in-water, $\eta \to 1$ and the reference command ϕ_r follows the operator input ϕ_{RC}. When the foil is out-of-water, it returns to neutral position $\theta \to 0$ since $I, \eta \to 0$ and $\phi_r = \phi$ in Equation (11).

V. Experimental Results

In this paper we present two experiments. The first experiment, displayed in figures 7a and 7b, is performed at the design speed of 10 m/s. At this speed, the hydrofoil generates the target moment loading of 1 Nm (lift of 6.6 N) with an angle of attack of 1.0°. As is shown in the figure, the experiment starts at a velocity of 7 m/s. The hydrofoil is lowered into the water and upon immersion, a loading command is issued to the system for about 80 seconds. Over the course of the run, the towing boat accelerates up to 10 m/s. Despite large variations in hydrofoil immersion height from $\sim$ 3 to 20 cm on a wide range or timescales, the commanded loading is followed, with an overall relative standard deviation error of 0.22. Generally, the load is maintained between 0.7 and 1.3 Nm and never exceeds 2 Nm. Overall, the control strategy is adequate for the objectives of interest.

The second experiment, carried out at low speed (4 to 6 m/s) is reported on Figure 7c. At 4 m/s, the 10 cm immersed hydrofoil would generate the 1 Nm target moment at an angle of attack of 6.5°. As is shown in the figure, the experiment is composed of two immersion events. Both times, the reference moment is well followed for some time, until a sudden loss of lift occurs (near 39 and 98 s). Visual inspection of the video recordings (Figure 8) shows that loss of lift is caused by a rapid inception of ventilation (note that if the absolute yaw of the vehicle is unknown, inferring whether the foil is ventilated of not is not easy *a priori*). When ventilation occurs, the controller increases the pitch of the foil and is successful at maintaining the desired load, albeit at a much higher angle of attack (it is qualitatively consistent with the fact that the lift slope for ventilated foils is 1/4 that of fully wetted foils). However, even though it is stable, this state of operation is not desirable as ventilation is associated with a large drag. Ventilation inception is favored by large angles of attack and flow separation. At low speeds, fulfilling the demanded loading requires such large angles of attack. In both occurrences, after the development of ventilation reducing the commanded loading to 0 or negative values helps closing the cavity—consistent with the hysteresis behavior of ventilation. At low speeds, limiting the demanded angle of attack may mitigate the likelihood of ventilation inception.

VI. Conclusions

Surface-piercing hydrofoils constitute an attractive actuator for high-speed, small-scale, and super-maneuverable surface vehicles, as they allow for the efficient generation of large forces. However, they come with unique challenges. Because of their small size and need to operate in waves, the hydrofoils must be slender and flexibility dominates their dynamics, while rapid changes in immersion height (similar

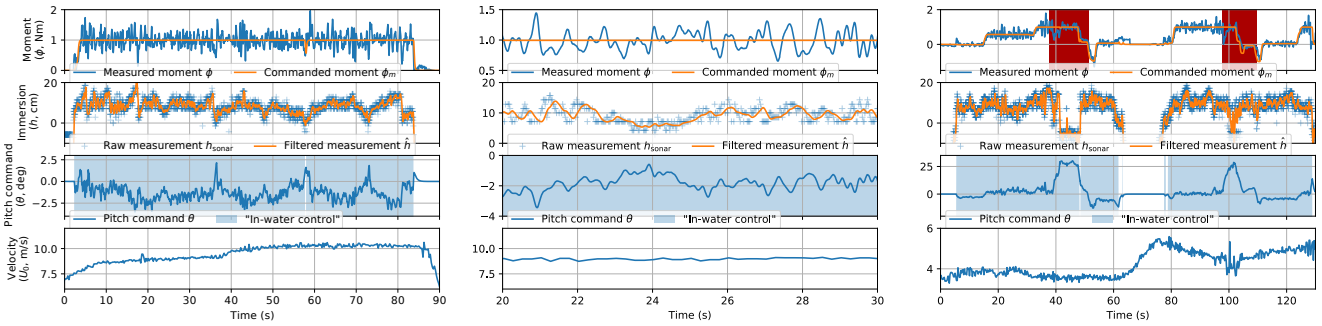

(a) (b) (c)

Fig. 7. (a) High-speed experiment. Despite significant speed variations between 8 and 10 m/s, and immersion height variation between $\sim$ 3 and 20 cm, and high-frequency wave forcing, the proposed controller is successful at maintaining the commanded loading. (b) Zoomed-in view of Figure 7a. (c) Low-speed experiment. As in Figure 7a, despite significant variations in speed and immersion height, command following is satisfactory. Two ventilation events are indicated with red background. Those events start with a loss of lift that is compensated by a large increase in hydrofoil pitch. Note that, because ventilation "opens" the water, during those events the sonar is unable to detect the water surface.

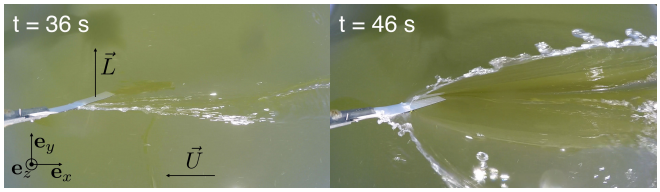

Fig. 8. Top-view of the hydrofoil in the low-speed experiment of Figure 7c. In the two instances, the lift generated is approximately the same. At t = 36 s the hydrofoil is fully wetted. At t = 46 s, after ventilation inception, a stable cavity has appeared. Ventilated flows are associated with large drag.

to a rapid change of the effective span, as in *e.g.* wing morphing) make for a highly time-varying plant. Finally, surface-piercing hydrofoils are potentially subject to ventilation – a phenomenon where atmospheric air is suddenly entrained into the suction side of the foil, provoking a loss of lift and increase in drag.

We designed and tested experimentally a LTV/feedback linearization load controller for a pitch-actuated, vertical, surface-piercing hydrofoil. The controller models lift forces with a panel method and utilizes speed and immersion depth measurements. It was successfully tested over a wide range of travel speeds and immersion depths. At low speed, when the commanded angle of attack is large, the system is prone to ventilation, limiting the amount of force that can be efficiently generated.

Acknowledgements

We thank Michael Novitzky, Hugh Dougherty and Michael Benjamin from the LAMSS, as well as Stewart Craig from the MIT Sailing Pavilion for their help with the experiments. We thank the reviewers for constructive remarks.

References

[1] C. C. Eriksen, T. J. Osse, R. D. Light, T. Wen, T. W. Lehman, P. L. Sabin, J. W. Ballard, and A. M. Chiodi, "Seaglider: A long-range autonomous underwater vehicle for oceanographic research," *IEEE Journal of Oceanic Engineering*, vol. 26, no. 4, pp. 424–436, 2001.

[2] R. P. Stokey, A. Roup, C. Von Alt, B. Allen, N. Forrester, T. Austin, R. Goldsborough, M. Purcell, F. Jaffre, G. Packard, and A. Kukulya, "Development of the REMUS 600 autonomous underwater vehicle," in *OCEANS*. Washington, DC: IEEE, 2005.

[3] J. Manley and S. Willcox, "The wave glider: A persistent platform for ocean science," in *OCEANS*. Sidney, Australia: IEEE, 2010.

[4] C. Meinig, N. Lawrence-Slavas, R. Jenkins, and H. M. Tabisola, "The Use of Saildrones to Examine Spring Conditions in the Bering Sea: Vehicle Specification and Mission Performance," in *OCEANS*. Washington, DC: IEEE, 2015.

[5] J. N. Newman, *Marine hydrodynamics*. MIT press, 1977.

[6] S. F. Hoerner, *Fluid-Dynamic Drag*. Published by the author, 1965.

[7] A. J. Acosta, "Hydrofoils and hydrofoil craft," *Annual Review of Fluid Mechanics*, vol. 5, 1973.

[8] O. M. Faltinsen, *Hydrodynamics of High Speed Marine Vehicles*. Cambridge University Press, 2005.

[9] T. Barden and J. Binns, "On the Road to Establishing Ventilation Probability for Moth Sailing Dinghies," *18th Australasian Fluid Mechanics Conference*, no. December, 2012.

[10] D. P. J. Hull, "Speed Sailing Design & Velocity Prediction Program," *Naval Engineers Journal*, vol. 127, no. 1, pp. 37–48, 2015.

[11] P. Conti and F. Rocchibi, "A Real-Time Simulator of Foiling Catamarans," pp. 57–70, 2014.

[12] J. Davenport, "How and why do flying fish fly?" *Reviews in Fish Biology and Fisheries*, vol. 4, no. 2, pp. 184–214, 1994.

[13] Y. L. Young, C. M. Harwood, F. Miguel Montero, J. C. Ward, and S. L. Ceccio, "Ventilation of Lifting Bodies: Review of the Physics and Discussion of Scaling Effects," *Applied Mechanics Reviews*, vol. 69, 2017.

[14] P. D. Swales, a. J. Wright, R. C. McGregor, and R. Rothblum, "The mechanism of ventilation inception on surface piercing foils," *Journal of Mechanical Engineering Science*, vol. 16, no. 1, pp. 18–24, 1974.

[15] S.-h. Kim and H. Yamato, "On the design of a longitudinal motion control system of a fully-submerged hydrofoil craft based on the optimal preview servo system," *Ocean*, vol. 31, pp. 1637–1653, 2004.

[16] P. Brisset, A. Drouin, M. Gorraz, P.-s. Huard, and J. Tyler, "The Paparazzi Solution," in *MAV 2006, 2nd US-European Competition and Workshop on Micro Air Vehicles*, 2006.

[17] G. Hattenberger, M. Bronz, and M. Gorraz, "Using the Paparazzi UAV System for Scientific Research," *IMAV 2014, International Micro Air Vehicle Conference and Competition 2014*, pp. 247–252, 2014.

[18] M. Drela, *Flight Vehicle Aerodynamics*. MIT press, 2014.

[19] H. Xü, "Potential flow solution for a yawed surface-piercing plate," *Journal of Fluid Mechanics*, vol. 226, pp. 291–317, 1991.

[20] Y. L. Young and S. Brizzolara, "Numerical and Physical Investigation of a Surface-Piercing Hydrofoil," in *International Symposium on Marine Propulsors*, no. May, Lanceston, Tasmania, Australia, 2013, pp. 1–8.

[21] M. Drela and H. Youngren, "AVL (Athena Vortex Lattice)," 2007.